COMMUNICATION

Controlled porous structures of graphene aerogels and their effect on supercapacitor performance†

Sung Mi Jung,[a] Daniela Lopes Mafra,[a] Cheng-Te Lin,[b] Hyun Young Jung*[c] and Jing Kong*[a]

The design and optimization of 3D graphene nanostructures are critically important since the properties of electrochemical energy storages such as supercapacitors can be dramatically enhanced by tunable porous channels. In this work, we have developed porous graphene aerogels from graphene suspensions obtained *via* electrochemical exfoliation and explored their application as supercapacitor electrodes. By adjusting the content of the electrolyte in the exfoliation process, the aspect ratio of graphene sheets and the porosity of the graphene network can be optimized. Furthermore, the freezing temperature in the freeze drying step is also found to play a critical role in the resulting pore size distributions of the porous networks. The optimized conditions lead to meso- and macroporous graphene aerogels with a high specific surface area, extremely low densities and superior electrical properties. As a result, the graphene aerogel supercapacitors exhibit a specific capacitance of 325 F g^{-1} at 1 A g^{-1} and an energy density of 45 Wh kg^{-1} in a 0.5 M H$_2$SO$_4$ aqueous electrolyte with high electrochemical stability and electrode uniformity required for practical usage. This research provides a practical method for lightweight, high-performance and low-cost materials in the effective use of energy storage systems.

Porous graphene materials have attracted vast attention due to their large theoretical surface area (2600 m^2 g^{-1}), unique porous structures, and excellent electrical conductivity.[1–4] These extraordinary features enable porous graphene materials to serve as key components in high-performance supercapacitors with their highly open porous structures allowing electrolytes access to the surface of porous frameworks.[5–7] Most porous graphene materials are derived from graphene oxide (GO) or reduced GO (rGO);[8–15] however, in many cases pristine graphene structures are more desirable.

We have previously produced the porous graphene aerogel from pristine graphene suspension obtained by using a surfactant and sonication assisted solution exfoliation.[16] Graphite flakes were first exfoliated with a surfactant in DI water using ultra-sonication at a dilute concentration, and then the suspension was transformed into a graphene gel by evaporating the solvent to reach the gel formation concentration ($\varphi_{gel} = a_r^{-1}$, where a_r is the aspect ratio of graphene nanosheet: $a_r = L/t$, and L is the lateral size and t is the thickness).[16] Nevertheless, for this method, the yield of the graphene nanosheet is limited, making it difficult for large scale production of porous networks. Furthermore, extensive sonication tends to result in graphene sheets of very small lateral size (hundreds of nanometers) and lower aspect ratio, which would require higher gel formation concentration to form a gel, as a result, the porous networks' properties (high density, low porosity, *etc.*) and performances in applications become limited.

During the past several years, electrochemical exfoliation of graphite has also been developed which allows the simple and large scale production of graphene sheets with more pristine qualities than rGO.[8–15] These graphene sheets are produced in aqueous solution at relatively high concentrations without the use of surfactants, with large lateral sizes (several micrometers) and thickness (~few layers), which greatly facilitate the formation of 3D graphene network structures of hydrogels and aerogels.

In this work, we produced highly conductive and porous graphene aerogels from graphene suspension obtained by using the electrochemical exfoliation and explored the application of these aerogels as electrodes for supercapacitors. We have found that the pore structure of graphene aerogels can be designed and optimized by tuning the aspect ratio of graphene sheets through adjustment of the exfoliation condition. Furthermore, the freeze drying temperature is also found to play a critical role in the resulting pore size distribution of the graphene structure. The optimized graphene aerogels have very low density, higher porosity and surface area, with pore sizes

[a]Department of Electrical Engineering and Computer Sciences, Massachusetts Institute of Technology, 77 Massachusetts Avenue, Cambridge, MA 02139, USA. E-mail: jingkong@mit.edu
[b]Department of Mechanical Engineering, Massachusetts Institute of Technology, 77 Massachusetts Avenue, Cambridge, MA 02139, USA
[c]Department of Mechanical and Industrial Engineering, Northeastern University, 360 Huntington Avenue, Boston, MA 02115, USA. E-mail: hjung@coe.neu.edu
†Electronic supplementary information (ESI) available. See DOI: 10.1039/c4nr07564a

ranging from several nanometers to several tens of micrometers, and remarkable electrical conductivity. The process here is very simple and allows large-scale production at a low cost. The study of supercapacitors using these electrodes has shown that such highly controlled meso- and macroporous structures of the graphene aerogels allow multidimensional electron transport and rapid electrolyte ion diffusion, which greatly enhanced the supercapacitor performances. Furthermore, electrodes made by this method demonstrate extraordinary structural stability and uniformity, which allows the construction of several supercapacitors in series and in parallel for practical usages.

We used the electrochemical exfoliation method to obtain high quality and large area thin graphene sheet suspensions for the formation of hydrogels and aerogels. Sulfuric acid (H_2SO_4) and potassium hydroxide (KOH) were used as electrolytes. The high concentration of H_2SO_4 solution affects exfoliation of graphites into much thinner graphene sheets, because SO_4^{2-} works as an intercalator in sulfuric acid, while the high acidity plays a major role to make defect on the graphene sheets. Therefore, KOH was added to reduce graphene oxidation by the acidic electrolyte (0.2 M H_2SO_4).[17,18] Alternating currents of ±1 A at 0.2 Hz were applied between the two graphite electrodes (Fig. S1a†). By using graphite as both electrodes (in contrast to graphite only as the anode previously), the exfoliation occurs at both electrodes resulting in higher exfoliation efficiency. The color change of the aqueous electrolyte solution from transparent to dark was observed after only a few minutes, indicating a high exfoliation rate and a very efficient process. These exfoliated graphene sheets were washed with DI water and then uniformly dispersed in ethanol without using any surfactant (Fig. S1b†). The resulting graphene suspension appears very homogeneous likely due to the presence of the functional groups on the graphene sheets and the remaining ions (such as SO_4^{2-}) in the suspension.[17]

The graphene gel was formed from interlinking of the graphene sheets by concentrating the uniformly dispersed graphene suspension up to the gel formation concentration (φ_{gel}). Here the gel formation concentration is lower than φ_{gel} made by sonication exfoliation[16] because the electrochemical exfoliation provides thinner and larger-area graphene sheets. Afterwards the gels were frozen at different freezing temperatures, and were transformed into graphene aerogels via the sublimation of the frozen solvent (ice) directly into water vapor. In order to obtain graphene sheets with a much higher aspect ratio (i.e., thinner in thickness and larger in area) so that aerogels with lower densities and better pore structures can be achieved, we tuned the aspect ratio by adding various amounts of KOH into the H_2SO_4 electrolyte (volume ratio of the original H_2SO_4 electrolyte : KOH solution = 9 : 1, with KOH having different concentrations: 23, 30, and 37 wt%)(Fig. 1a). It was observed that lower concentration of KOH results in a thinner but smaller exfoliated graphene sheet (Fig. S2†). The optimum aspect ratio is achieved with 30 wt% KOH (Fig. 1e), where large-area thin graphene sheets with 3.7 ± 1 μm lateral size (Fig. 1b) and 2.5 ± 0.1 nm thickness (Fig. 1c and Fig. S1c†) were obtained. Fig. 1d and e compare the graphene aerogels made from graphene sheets having two different aspect ratios
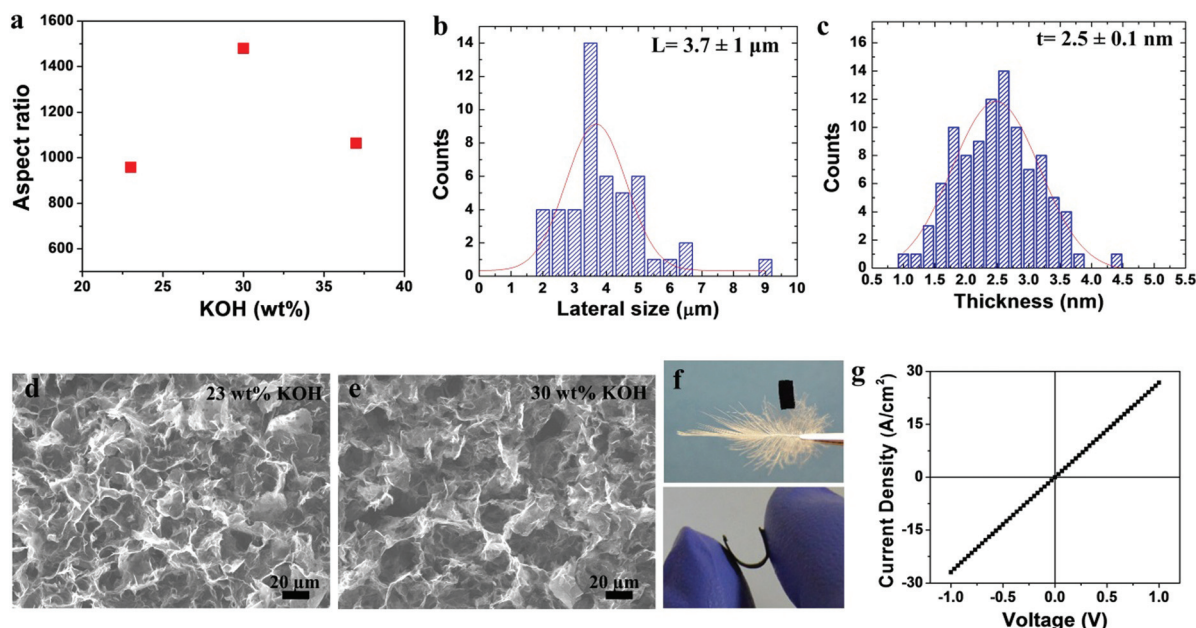

Fig. 1 (a) The aspect ratio of the exfoliated graphene sheets at 23, 30, and 37 wt% KOH in H_2SO_4 electrolyte. The sheet size (b) and thickness (c) distribution of exfoliated graphene for 30 wt% KOH in H_2SO_4 electrolyte. The average sheet size is about 3.7 ± 1 μm and the average thickness is 2.5 ± 0.1 nm. (d, e) SEM images of aerogels using graphene sheets exfoliated at 23 (d) and 30 (e) wt% KOH in H_2SO_4 electrolyte (−20 °C freezing temperature was used for the freeze drying step). (f) Optical pictures showing ultralight, flexible and bendable natures of as-prepared graphene aerogels (e). (g) I−V curve of the graphene aerogel in (e): electrical conductivity, σ = 509 S m^{-1}.

(aspect ratio of 958 from 23% KOH and aspect ratio of 1480 from 30% KOH; the rest processing conditions (such as freeze drying) are all the same). By comparing Fig. 1d and e, it can be seen that the aerogels made with larger aspect ratio graphene sheets have larger pore sizes. Furthermore, the graphene aerogel derived from the sheets made with 30% KOH has a density of 6.5 mg cm^{-3}, lower than the one made with 23% KOH (11.5 mg cm^{-3}). As a result, for the later part of the investigation, we focus on the aerogels made with graphene sheets produced by 30% KOH, which are ultralight, flexible and bendable (Fig. 1f). Fig. 1g shows the electrical measurement result of the graphene aerogel in Fig. 1e; an electrical conductivity of 509 S m^{-1} was obtained. Considering the density of this aerogel is only 6.5 mg cm^{-3}, this number is remarkable. As a comparison, a conductivity of 273 S m^{-1} with two times higher density (13 mg cm^{-3})[16] was obtained in our previous graphene aerogel using sonication exfoliated graphene, and a conductivity of 100 S m^{-1} with five times higher density (10 mg cm^{-3})[11] was obtained in graphene aerogel made by reduced graphene oxide. Such an extraordinary electrical characteristic suggests the high quality of not only the graphene network, but also the sheets obtained from the electrochemical exfoliation.

We have also found that the freeze drying temperature plays a critical role in the resulting porous morphology of the gra-

phene aerogels, similar to the recent finding by X. Xie *et al.*[8] The scanning electron microscopy (SEM) images in Fig. 2a–c show the morphology of graphene aerogels made at different freezing temperatures (−200 °C (Fig. 2a), −80 °C (Fig. 2b), and −20 °C (Fig. 2c)). These images reveal clearly that the freeze-dried graphene aerogels have an interconnected 3D macroporous network with pore sizes in the range of sub-micrometers to several tens of micrometers. On comparing among them, it shows that even though the same graphene gels were used before freeze drying, different freezing temperatures give rise to different morphologies of the graphene network. The macropore size increases as the freezing temperature increases and especially enlarges up to 60 μm at a high freezing temperature of −20 °C. Since the graphene gels were directly brought from room temperature to these freezing temperatures, different freezing temperatures imply different freezing (or ice solidifying) rates. At a low freezing temperature of −200 °C, a high freezing rate would imply a high nucleation rate of ice with low or no crystal growth.[8] This will result in large amount of ice crystals with small sizes, and the final graphene aerogels have small pore sizes.[10] On the other hand, at a high freezing temperature of −20 °C, the ice solidification rate is low, favoring crystal growth with less nucleation. This results in fewer ice crystals and larger crystal sizes. When the ice is removed *via* sublimation using a freeze dryer, larger
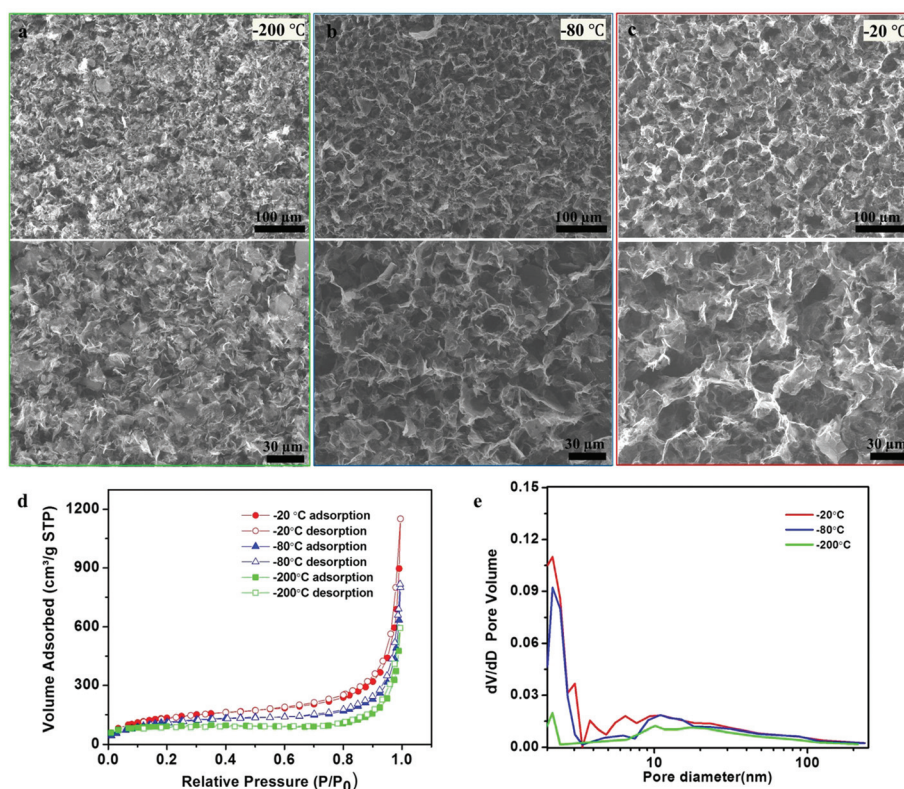

Fig. 2 SEM images of the graphene aerogels fabricated at freezing temperatures of −200 (a), −80 (b), and −20 °C (c). (d) N$_2$ adsorption−desorption isotherms of the freeze-dried graphene aerogels at −20, −80, and −200 °C, with 504, 441, and 315 m^2 g^{-1} of specific surface areas calculated respectively by the Brunauer−Ennett−Teller (BET) method, and (e) pore size distribution of graphene aerogel made at different freezing temperatures.

crystal sizes result in networks with larger pore sizes. Therefore, since the freezing rate controls the nucleation and growth of ice crystals, the freezing temperature become the critical factor for determining the morphology of the macropores in the aerogel.[8]

The mesoporous structures of the graphene networks were further verified by N_2 adsorption–desorption analysis. In Fig. 2d, all the aerogels fabricated at the different freezing temperatures showed a type IV isotherm with a H3-type hysteresis loop, which indicates that mesopores have cylindrical pore geometries.[19] The aerogel made at higher freezing temperature shows a higher absorbed volume, corresponding to a larger specific surface area. The specific surface areas of these aerogels were calculated as 504, 441, and 315 $m^2 g^{-1}$ for the freezing temperatures −20 °C, −80 °C, −200 °C respectively by the Brunauer–Ennett–Teller (BET) method (Fig. 2d). Fig. 2e shows the pore size distribution of the graphene aerogels made at three different temperatures. The aerogel made at −20 °C shows the highest pore volume with the pore diameter range of 2 to 50 nm (mesopores). Combined with the SEM images showing larger than micrometer sized pores, we conclude that our aerogels possess hybrid structures consisted of both mesopores and macropores, with the −20 °C sample possessing the largest volume in both types of pores. As a comparison with the recent development of a porous graphene structure with an exceptionally high specific surface area (3523 $m^2 g^{-1}$),[10] although the specific surface area of our graphene aerogels here is 6–10 times lower, the specific capacitance (shown later) is actually higher under the same measurement conditions. This indicates that even though the surface area plays an important role in the capacitor performance, the porous structure (such as having both types of pores (mesopores and macropores)) also plays a critical role, because combination of the two types of pores ensures effective transportation of ions.[20]

We have carried out electrochemical measurements to study the performance of these porous graphene aerogels as electrodes in electrical double-layer capacitors (EDLCs). The graphene aerogels with different porosities from three freezing temperatures serve as the anode and the cathode, mechanically separated by a piece of cotton paper as the separator, which are electrically connected to each other *via* the electrolyte. The small mesopores within the interconnected macroporous network of the aerogels are expected to provide high permeability to electrolyte ions. Cyclic voltammetry (CV) was performed to evaluate the capacitance of the graphene aerogel (−20, −80, and −200 °C) supercapacitors with all three different porosities in the 0.5 M H_2SO_4 electrolyte. The CV curves of the graphene aerogel supercapacitors were measured with various scan rates in the range of 20–500 $mV s^{-1}$. All CV curves show a very rapid current response to the voltage reversal at each end potential. The rectangular shapes of these curves indicate a very small equivalent series resistance of electrodes, corresponding to fast ionic diffusion in the electrolyte. Particularly for the case of the aerogel freeze dried at −20 °C (Fig. 3a), nearly rectangular shaped CV curves were obtained

even at very high scan rates, demonstrating high performance capacitor devices (for the devices in freezing temperatures from −80 and −200 °C, see Fig. S3a and S3b†). Fig. 3b shows the capacitance calculated from the CV curves as a function of the freezing temperatures and scan rates. The capacitance increased as the scan rates decreased, and the graphene aerogel fabricated at −20 °C freezing temperature has the highest capacitance of 255 $F g^{-1}$ at a scan rate of 20 $mV s^{-1}$.

Fig. 3c shows the galvanostatic charge/discharge (CD) conducted at different current densities to evaluate the specific capacitance and internal resistance of the graphene aerogel supercapacitor device (for the devices in freezing temperatures from −80 and −200 °C, see Fig. S3c and S3d†). The E–t responses of the charge process show a nearly triangular shape and mirror image with the corresponding discharge counterparts confirming the formation of an efficient capacitor and excellent charge propagation across two electrodes. The specific capacitances calculated from discharge curves are 125, 230, and 325 $F g^{-1}$ at 1 $A g^{-1}$ for graphene aerogel supercapacitors made at −200, −80, and −20 °C freezing temperatures, respectively (Fig. 3d). For the graphene aerogel supercapacitor of −20 °C freezing temperature, where electrochemically active surface and porosity are maximized, the measured specific capacity is 2.6 times higher than −200 °C graphene device and 1.35–1.7 times and 1.4 times higher than 3D graphene supercapacitors in aqueous[21,22] and ionic liquid[10] electrolytes, respectively.

Fig. 3e compares energy densities calculated from the CD curves as a function of discharge current density. Energy density increases with decreasing current density, and has the highest value of 45 $Wh kg^{-1}$ from the aerogel obtained at −20 °C freezing temperature. The high freezing temperature greatly improves electrochemical performances of the graphene aerogel supercapacitor due to the more effective combination of interconnected mesopores and macropores in aerogels. The mesopores are essential for high energy storage[20] and furthermore macropores in graphene aerogels can accelerate the kinetic process of ion diffusion. Therefore, our method to tailor pore sizes in the macropore regime with mesopore sizes suggests effective direction for high performance supercapacitors.

To evaluate energy storage performance of graphene aerogel devices, energy densities are plotted *versus* power density (Ragone plot) as shown in Fig. 3f. The gravimetric energy density of the graphene aerogel-based supercapacitor fabricated at −20 °C shows a higher value than the graphene aerogel devices at −80 and −200 °C freezing temperatures. This remarkable capacitor behavior can be attributed to the well-controlled pore size features on the electrode, the increased surface area, and the maximized active electrochemical surface area and hybrid porosity. The Ragone plots are also compared with carbon-based supercapacitors performed in H_2SO_4 electrolyte.[23–29] The maximum energy density of the graphene aerogel-based supercapacitor is 45 $Wh kg^{-1}$. This value is significantly higher than that of other supercapacitors. The power density of graphene aerogel devices is still higher
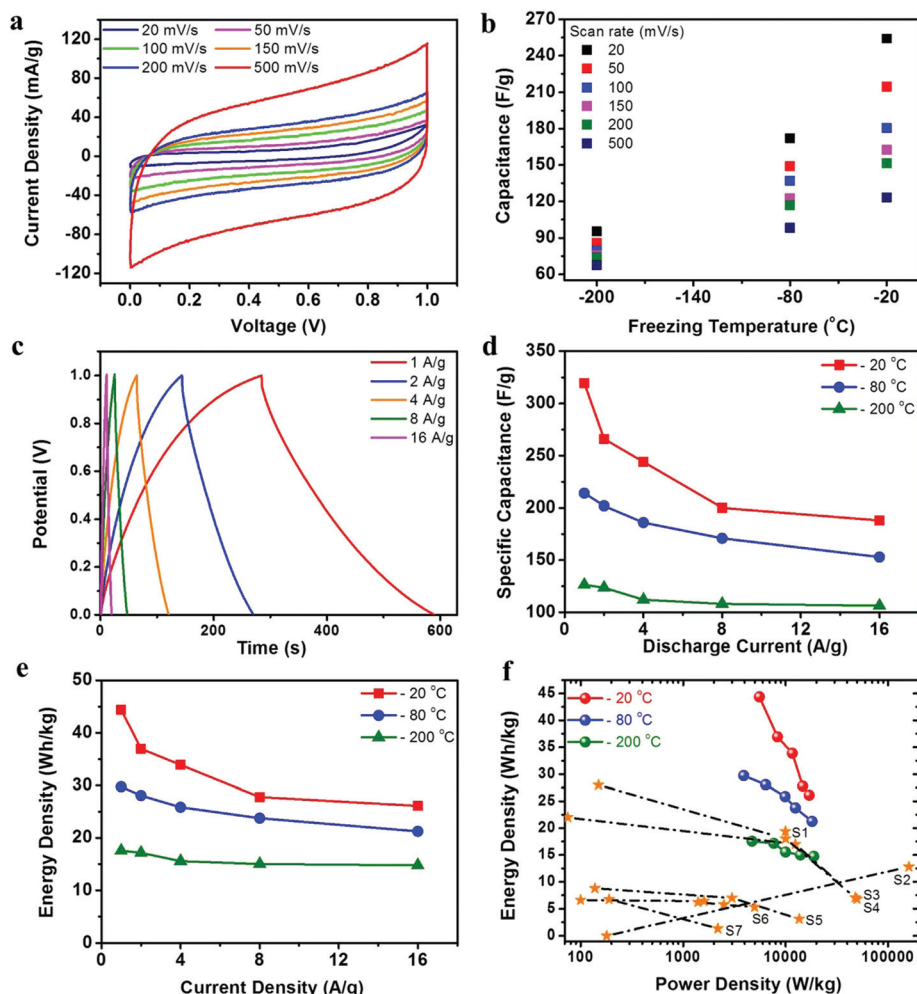
Fig. 3 (a) The CV curves of the graphene aerogel (freezing temperature of −20 °C) supercapacitors measured at various scan rates between 20 and 500 mV s⁻¹. (b) The capacitance calculated from CV curves as a function of freezing temperatures and scan rates. (c) Galvanostatic charge/discharge curves of the graphene aerogel (freezing temperature of −20 °C) supercapacitors measured at different current densities. (d) Specific capacitances of samples made at different freezing temperatures calculated from CD curves as a function of the discharge current. (e) Energy densities calculated from the CD curves as a function of discharge current density. (f) Ragone plot of the graphene aerogel samples in this work compared to previous studies (S1–S7[23−29]).

than that of the most of other supercapacitors. Although some show larger power density than ours, those were performed in 10 times higher concentration H_2SO_4 electrolyte of 5 M (S2),[24] or at a high measurement temperature of 60 °C (S3)[25] causing irreversible redox reactions or by using metal oxide (RuO_2) assistants and a polyaniline pseudocapacitor (S4).[26] As far as we know, the combination of the energy density and power density of the graphene aerogel electrodes shows excellent performance, and is among the best reported values for EDLCs using an aqueous electrolyte.

In general, the total energy that can be stored in a single supercapacitor is not enough for many applications. To further demonstrate the practical usage and the reliability of the high performance supercapacitors based on graphene aerogels, we connected three supercapacitor units in series to create a tandem device. Each supercapacitor unit has the same mass loading of graphene aerogels fabricated at −20 °C freezing

temperature. Cyclic voltammetry in Fig. 4a was performed at a scan rate of 50 mV s⁻¹ and its potential window extends to 4.0 V for such a tandem device. A voltage scan in the range from 0.8 to 3.6 V did not reveal any significant increase of anodic current, even though a small increase of the measured current can be observed during scanning. It means that the electrolyte is not being decomposed, where the minimum decomposition voltage of water at 25 °C is about 1.25 V. The practical voltage of over 3 V can be successfully applied to a capacitor operating in this electrolyte. The adaptability of graphene aerogel supercapacitors for galvanostatic charge/discharge cycling is demonstrated by connecting three devices together both in series and in parallel configurations (Fig. 4b–c). Galvanostatic cycling was performed at a current density of 1 A g⁻¹ and 2 A g⁻¹ for series and parallel connections, respectively. Similar to the individual units, the tandem devices exhibit nearly ideal triangular charge/discharge curves which
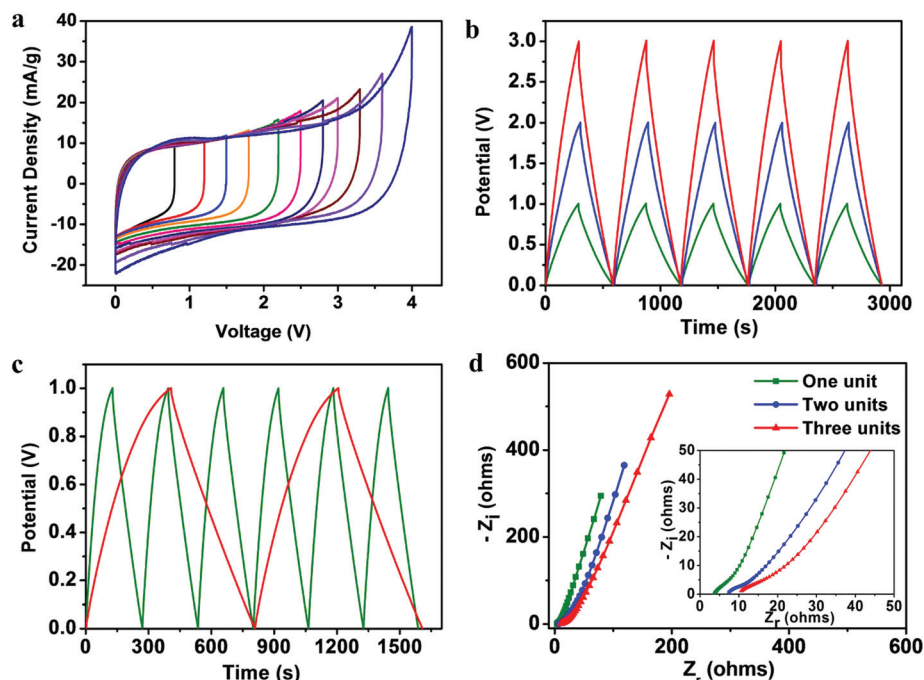
Fig. 4 (a) CV curves of a unit with three supercapacitors in series at a scan rate of 50 mV s^{-1}. Here the same colors represent single cycle scanned to a particular voltage range (0.8, 1.2, 1.5, 1.8, 2.2, 2.5, 2.8, 3.0, 3.3, 3.6, 4.0 V, respectively). (b, c) Galvanostatic charge/discharge curves of super-capacitors in series (b) and in parallel (c) connection. The current density is 1 A g^{-1} for series connection ((b), green, blue and red solid line are one, two and three unit cells, respectively) and 2 A g^{-1} for parallel connection ((c), green and red are one and three parallel cells respectively). (d) Electro-chemical impedance spectroscopy of a graphene aerogle electrode in the frequency range from 10 mHz to 100 kHz.

indicate excellent capacitive properties. In particular, in series connection, the device shows practically unchanged charge/discharge time, suggesting that the performance of each supercapacitor unit is well retained in series and parallel connections.

Electrochemical impedance spectroscopy in the frequency range from 10 mHz to 100 kHz was performed to confirm the superior performance of the graphene aerogel supercapacitor. From the curve shape of the impedance measurement, a pore geometry can be derived, and the result of V-shaped pore geometries was observed from all the device units.[30] Such a shape would imply that small ions can permeate through all electrode surfaces without obstruction and constrain, which explains the reason for the high performance of these aerogel electrodes. The equivalent series resistance obtained at the highest frequency (100 kHz) on the real axis is only 3.6 Ω for one supercapacitor unit and 10.7 Ω for three units, which directly proves that the charge transfer at the electrode–electrolyte interface is very quick and current can pass very easily through the interface with low internal resistance. Finally we measured the long cycle life (number of charge–discharge cycles at constant current) of three tandem super-capacitors. The normalized capacitance and the coulombic efficiency as a function of cycle-number are shown in Fig. 5. The supercapacitor devices show long life cycle stability: >98% coulombic efficiency of the initial capacitance after 5000 cycles, allowing practical applications for high power and high voltage operation.
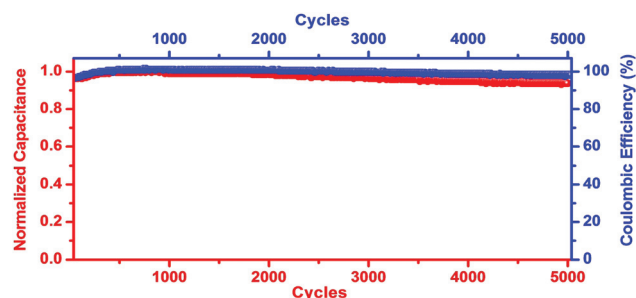

Fig. 5 The normalized capacitance and coulombic efficiency of a unit with three tandem supercapacitors during 5000 cycles.

In conclusion, we have demonstrated the design of graphene aerogel supercapacitors with high performance from the electrochemically exfoliated larger-area thin graphene sheet suspensions. Compared with other methods to achieve graphene solutions, the electrochemical exfoliation has high throughput and scalability, and the produced graphene sheets have high aspect ratio and quality. These characteristics facilitate the production bulk porous graphene structures at a large scale with low cost. We have also found that the aspect ratios of the graphene flakes can be optimized by tuning the conditions during the electrochemical exfoliation. This allows the optimization of the structures in the graphene aerogel to achieve the best performances in their applications. Furthermore, the porous structure of graphene aerogels can also be tuned by the freezing temperature in the freeze drying process.

The unique morphological and structural features of the graphene aerogels maximize the active electrochemical surface area and porosity, leading to high energy storage performance. In particular, interconnected meso- and macropores of graphene aerogels can provide fast ion channels to facilitate ion transport for high performance. The graphene electrodes obtained from this method demonstrate excellent uniformity and stability, which allow the construction of cells in parallel and series, enabling the high voltage operation even with an aqueous electrolyte. Combining with the efficient and low cost production of graphene solutions from the electrochemical exfoliation, our work here demonstrates a feasible route for graphite powder in practical energy storage applications.

Experimental section

Fabrication of graphene suspensions

The graphene suspension with high-quality thin graphene sheets was obtained by electrochemical exfoliation of natural graphite flakes.[17] For the electrochemical exfoliation, two graphite electrodes were immersed into the electrolyte solution as an anode and a cathode. In order to minimize graphene oxidation by the acidic electrolyte (0.2 M sulfuric acid (H_2SO_4)), different concentrations (23, 30, and 37 wt%) of potassium hydroxide (KOH) were added to obtain the optimized result with the largest aspect ratio (lateral dimension: thickness) of the graphene sheets, and uniform dispersion of graphene without any surfactant at high concentration. The electrochemical exfoliation process was carried out by applying alternating current (±1 A) with a duration time of 5 seconds for each. As a result, the graphene sheets were exfoliated alternatively from one graphite electrode at 10–15 V. The exfoliated graphene sheets were collected with a 100 nm porous filter and washed with DI water by filtration. Then, the exfoliated graphene sheets were uniformly dispersed in ethanol.

Fabrication of graphene aerogels

The aerogel fabrication is based on our previous study[16] *via* the assembly of anisotropic nano-objects into a cross-linking network from their colloidal suspensions at the transition from the semi-dilute to the isotropic concentrated regime. The thickness and sheet size of the exfoliated graphene optimized to fabricate the graphene aerogel were about 2.5 nm and 3.7 μm at 30 wt% KOH in H_2SO_4 aqueous solution. The dilute suspensions of the exfoliated graphene were evaporated slowly at 313 K to transform them into more concentrated suspensions (gels) with a large volume compression. As the concentration increases, some graphene sheets come physically in contact with each other through van der Waals forces, and at higher concentrations a 3D network is formed by these interconnected branches composed of graphene sheets and thus a graphene gel is obtained. After that, ethanol in the pore of the gel was exchanged with DI water, which is then removed *via* freeze-drying. For the freeze drying process, the graphene gels were first frozen at different temperatures (−200 °C, −80 °C,

and −20 °C). The ice is removed by sublimation using a freeze dryer to ensure the porous network without shrinking or collapsing.

Property characterization

Atomic force microscopy (AFM, Dimension 3100, Veeco System) measurements were carried out to characterize the thickness and size of the graphene sheets. Scanning electron microscopy (JEOL 6700F) was used to characterize the porosities of the aerogel networks. Nitrogen adsorption and desorption isotherms for the porosities of the aerogels were measured at 77 K on a Micromeritics ASAP 2010 system. Before the measurement, the samples were degassed at 423 K under vacuum (<10^{-4} mbar) for several hours. Surface areas of the aerogels were calculated by the Brunauer–Ennett–Teller (BET) method with a multi-molecular layer adsorption model. The electrical conductivities of the graphene aerogel at room temperature were measured using a four-probe station for porous materials. The resulting errors in the electrical conductivity measurement were estimated to be less than 5%.

Characterization of supercapacitor devices

The graphene aerogels were used directly as anodes and cathodes for assembling symmetric supercapacitors in 0.5 M H_2SO_4 aqueous electrolyte. The electrochemical properties of graphene aerogel-based supercapacitors were analyzed using cyclic voltammetry (CV), galvanostatic charge–discharge (CD), electrochemical impedance spectroscopy (EIS) and cyclic stability by Potentiostat (VersaSTAT 4) at room temperature. The CV curves were measured between 0 and 1 V for one unit supercapacitor in the 0.5 M H_2SO_4 electrolyte with various scan rates in the range of 10–500 mV s^{-1} and between 0 and 4 V for three tandem supercapacitors. To quantitatively evaluate the charge storage capacity at each scan rate, the capacitance of the graphene aerogel is calculated based on the following method:[31] $C = \int_{E_1}^{E_2} i(E)\mathrm{d}E/2(E_2 - E_1)mv$, where C is the capacitance of the sample, E_1, E_2 are the cutoff potentials in the cyclic voltammetry, $i(E)$ is the instantaneous current, $C = \int_{E_1}^{E_2} i(E)\mathrm{d}E$ is the total voltammetric charge obtained by integration of positive and negative sweeps in cyclic voltammograms, $(E_2 - E_1)$ is the potential window width, and m is the mass of a single electrode. The CD curves are obtained at a constant current density in the range of 1 to 20 A g^{-1}. The capacitance and internal resistance values are determined from the slope and the initial voltage drop of the galvanostatic CD curves, respectively. The specific capacitances, C_s, are calculated from the galvanostatic discharge curves[32] using $C_s = i/-[\Delta V/\Delta t]m = i/-\text{slope} \times m$, where i is the discharge current, and the slope is the slope of the discharge curve after the iR drop. For EIS, the amplitude of the AC signal applied to the electrodes was 50 mV and the frequency was varied from 10 mHz to 100 kHz. The efficiency (η), the power density (P) and the energy density (E) are calculated using $\eta = (t_d/t_c) \times 100$, $P = V^2/[4Rm]$ and $E = 0.5CV^2/m$, respectively where t_d is the discharging time, t_c is the charging time, and R is the internal resistance, respectively.

Acknowledgements

References

1 A. Peigney, C. Laurent, E. Flahaut, R. R. Bacsa and A. Rousset, *Carbon*, 2001, **39**, 507.

2 S. Han, D. Wu, S. Li, F. Zhang and X. Feng, *Adv. Mater.*, 2014, **26**, 849.

3 A. K. Geim and K. S. Novoselov, *Nat. Mater.*, 2007, **6**, 183.

4 Z. Chen, W. Ren, L. Gao, B. Liu, S. Pei and H.-M. Cheng, *Nat. Mater.*, 2011, **10**, 424.

5 J. Hu, Z. Kang, F. Li and X. Huang, *Carbon*, 2014, **67**, 221.

6 F. Zeng, Y. Kuang, G. Liu, R. Liu, Z. Huang, C. Fu and H. Zhou, *Nanoscale*, 2012, **4**, 3997.

7 D. Brownson, D. K. Kampouris and C. E. Banks, *J. Power Sources*, 2011, **196**, 4873.

8 X. Xie, Y. Zhou, H. Bi, K. Yin, S. Wan and L. Sun, *Sci. Rep.*, 2013, **3**, 2117.

9 C. Li and G. Shi, *Nanoscale*, 2012, **4**, 5549.

10 L. Zhang, F. Zhang, X. Yang, G. Long, Y. Wu, T. Zhang, K. Leng, Y. Huang, Y. Ma, A. Yu and Y. Chen, *Sci. Rep.*, 2013, **3**, 1408.

11 M. A. Worsley, P. J. Pauzauskie, T. Y. Olson, J. Biener, J. H. Satcher and T. F. Baumann, *J. Am. Chem. Soc.*, 2010, **132**, 14067.

12 G.-N. Cristina, R. T. Weitz, A. M. Bittner, M. Scolari, A. Mews, M. Burghard and K. Kern, *Nano Lett.*, 2007, **7**, 3499.

13 J. Zou and F. Kim, *Nat. Commun.*, 2012, **3**, 1241.

14 L. Qiu, J. Z. Liu, S. L. Y. Chang, Y. Wu and D. Li, *Nat. Commun.*, 2014, **5**, 5254.

15 W. Ouyang, J. Sun, J. Memon, C. Wang, J. Geng and Y. Huang, *Carbon*, 2013, **62**, 501.

16 S. M. Jung, H. Y. Jung, M. S. Dresselhaus, Y. J. Jung and J. Kong, *Sci. Rep.*, 2012, **2**, 849.

17 C. Y. Su, A. Y. Lu, Y. P. Xu, F. R. Chen, A. N. Khlobystov and L. J. Li, *ACS Nano*, 2011, **5**, 2332.

18 K. Parvez, Z.-S. Wu, R. Li, X. Liu, R. Graf, X. Feng and K. Müllen, *J. Am. Chem. Soc.*, 2014, **136**, 6083.

19 S. J. Gregg and K. S. W. Sing, *Adsorption, Surface Area and Porosity*, Academic Press, New York, 1982.

20 T. Y. Kim, G. Jung, S. Yoo, K. S. Suh and R. S. Ruoff, *ACS Nano*, 2013, **7**, 6899.

21 Y. Xu, Z. Lin, X. Huang, Y. Wang, Y. Huang and X. Duan, *Adv. Mater.*, 2013, **25**, 5779.

22 Y. Xu, K. Sheng, C. Li and G. Shi, *ACS Nano*, 2010, **4**, 4324.

23 W. Wang, Q. Hao, W. Lei, X. Xia and X. Wang, *RSC Adv.*, 2012, **2**, 10268.

24 H. Zhang, V. V. Bhat, N. C. Gallego and C. I. Contescu, *ACS Appl. Mater. Interfaces*, 2012, **4**, 3239.

25 Z. Xu, Z. Li, C. Holt, X. Tan, H. Wang, B. S. Amirkhiz, T. Stephenson and D. Mitlin, *J. Phys. Chem. Lett.*, 2012, **3**, 2928.

26 J. Zhang, J. Jiang, H. Li and X. S. Zhao, *Energy Environ. Sci.*, 2011, **4**, 4009.

27 D. Puthusseri, V. Aravindan, S. Madhavi and S. Ogale, *Energy Environ. Sci.*, 2014, **7**, 728.

28 Y. Xu, Z. Liu, X. Huang, Y. Liu, Y. Huang and X. Duan, *ACS Nano*, 2013, **7**, 4042.

29 L. T. Le, M. H. Ervin, H. Qiu, B. E. Fuchs and W. Y. Lee, *Electrochem. Commun.*, 2011, **13**, 355.

30 H. Keiser, K. D. Beccu and M. A. Gutjahr, *Electrochim. Acta*, 1976, **21**, 539.

31 W. Chen, Z. Fan, L. Gu, X. Bao and C. Wang, *Chem. Commun.*, 2010, **46**, 3905.

32 H. Y. Jung, M. B. Karimi, M. G. Hahm, P. M. Ajayan and Y. J. Jung, *Sci. Rep.*, 2012, **2**, 773.